

Stokes drag on a sphere in a three-dimensional anisotropic porous medium

Andrej Vilfan,^{1,*} Bogdan Cichocki,^{2,†} and Jeffrey C. Everts^{2,3,‡}

¹*Jožef Stefan Institute, 1000 Ljubljana, Slovenia*

²*Institute of Theoretical Physics, Faculty of Physics,*

University of Warsaw, Pasteura 5, 02-093 Warsaw, Poland

³*Institute of Physical Chemistry, Polish Academy of Sciences, 01-224 Warsaw, Poland*

(Dated: April 29, 2025)

We study the hydrodynamic drag force exerted on a sphere in a static anisotropic porous medium. This problem is analysed using the Brinkman-Debye-Bueche equations with an axisymmetric shielding (or permeability) tensor. Using the exact Green's functions for this model fluid within a single-layer boundary element formulation, we numerically compute the friction tensor for a translating sphere subjected to stick boundary conditions. Furthermore, we derive approximate analytical expressions for small anisotropy using the Lorentz reciprocal theorem. By benchmarking this result against the numerical solutions, we find that a linear approximation is valid in a broad parameter regime. Our results are important for studying self-diffusion in general anisotropic porous media, but can also be applied to small tracers in nematic fluids composed of disk- or rod-like crowders.

I. INTRODUCTION

In soft matter and biology, liquids permeating porous media are often found due to the occurrence of (polymeric) fibres, membranes, and colloidal particles [1–5]. It is a key challenge to describe the flow through such systems – typically at a low Reynolds number – while also accounting for the precise porous microstructure of the medium [6–8]. Therefore, understanding the macroscale flow properties often requires a coarse-grained approach. In the Brinkman-Debye-Bueche (BDB) method [9, 10], the porous features of the system are represented by an effective mesoscopic medium that exerts an additional force density on the permeating fluid that is linear in the fluid velocity. Although this method has been widely studied [11] and applied [12–14], mostly isotropic effective media have been considered. Despite the possible profound effects of anisotropy [15, 16], there are only a few results available for BDB models where the pores or building blocks are, on average, aligned in a specific direction. Here, we want to address this issue in the context of self-diffusion of a spherical tracer.

The main motivation for studying this problem is a series of experiments by Kang *et al.* [17–19], where the long-time self-diffusion coefficient of a spherical tracer particle is determined in a network of nematically ordered rod-like particles. These experiments have been interpreted using effective medium theories based on cluster expansions incorporating rod-sphere hydrodynamic interactions [17–21], which are only valid for low volume fraction of rods on the level of the friction tensor. Furthermore, only isotropic hydrodynamic screening was included in the model, even in cases where the network of rods is nematic. In these works, the spherical tracers are

much smaller than the rod-like crowders and are thus not expected to distort the nematic host. Although confinement and crowding do not necessarily influence diffusion in the same manner [22], we can approximate the crowded environment of rods as an anisotropic porous medium for small enough tracer sizes. Therefore, an anisotropic BDB approach gives a different perspective on this problem and could correct the theories presented in Refs. [17–21].

A direct way to incorporate anisotropy in the BDB approach is to replace the shielding length (which is equivalent to the permeability) with a shielding tensor that reflects the spatial symmetry of the underlying porous mass [23]. For this case, the Green's functions have been analytically computed in two spatial dimensions [24] and later generalised to three spatial dimensions for axisymmetric systems up to one integral [25]. Such analytical expressions are important because they can be directly used in the Boundary Element Method (BEM) [26] to compute, for example, hydrodynamic drag forces.

This work focuses on the numerical and analytical computation of the Stokes drag force on a sphere suspended in an unbounded axisymmetric BDB fluid. The paper is organised as follows. In Sec. II, we describe the equations governing the flow in an anisotropic BDB fluid and present the corresponding Green's functions. Furthermore, we formulate the friction problem for a sphere in anisotropic BDB fluid, which is relevant for self-diffusion and hydrodynamic drag studies. In Sec. III, we analyze the friction problem for small anisotropy with the help of the Lorentz reciprocal theorem. In Sec. IV, we compute the friction tensor for arbitrary anisotropy using the BEM and compare the results with the analytical approximation of Sec. III. We present our conclusions and an outlook in Sec. V.

II. DESCRIPTION OF THE MODEL FLUID

We consider an incompressible, anisotropic BDB fluid, described by the (average) fluid velocity $\mathbf{v}(\mathbf{r})$ and pres-

* andrej.vilfan@ijs.si

† bogdan.cichocki@fuw.edu.pl

‡ jeffrey.everts@fuw.edu.pl

sure $p(\mathbf{r})$. Conservation of linear momentum and the incompressibility condition, respectively, give

$$\eta_{\text{eff}} \nabla^2 \mathbf{v}(\mathbf{r}) - \eta \boldsymbol{\kappa}^2 \cdot \mathbf{v}(\mathbf{r}) - \nabla p(\mathbf{r}) = -\mathbf{f}(\mathbf{r}), \quad (1)$$

$$\nabla \cdot \mathbf{v}(\mathbf{r}) = 0. \quad (2)$$

Here, η is the shear viscosity of the fluid in the porous mass, η_{eff} is the effective viscosity of the medium composed of the porous mass and the fluid, $\mathbf{f}(\mathbf{r})$ is a force density acting on the fluid, and $\boldsymbol{\kappa}$ is a spatially constant shielding tensor. Furthermore, we consider cylindrical (or “nematic”) symmetry of $\boldsymbol{\kappa}$,

$$\boldsymbol{\kappa} = \kappa_{\parallel} \hat{\mathbf{n}} \hat{\mathbf{n}} + \kappa_{\perp} (\mathbf{I} - \hat{\mathbf{n}} \hat{\mathbf{n}}), \quad (3)$$

with the axis of cylindrical symmetry $\hat{\mathbf{n}}$. Here, κ_{\parallel} and κ_{\perp} are inverse “screening” lengths parallel to $\hat{\mathbf{n}}$ and in the plane perpendicular to $\hat{\mathbf{n}}$, respectively.

The second term in Eq. (1) can be interpreted as an external force density exerted by the porous mass on the fluid. The precise form of this (Brinkman) damping force is chosen so that for small velocity gradients (or $\eta_{\text{eff}} = 0$) and $\mathbf{f} = \mathbf{0}$, the Darcy law is retrieved [27, 28]. Consequently, the inverse of $\boldsymbol{\kappa}^2$ can be interpreted as the permeability tensor of the porous mass. In this work, we take $\eta_{\text{eff}} = \eta$. Cases where $\eta_{\text{eff}} \neq \eta$ and non-zero can be taken into account by a suitable rescaling of $\boldsymbol{\kappa}$ depending on the problem of interest.

A. Point force response

The fundamental solution can be obtained by setting $\mathbf{f}(\mathbf{r}) = \mathbf{F}_p \delta(\mathbf{r})$. By linearity of Eqs. (1) and (2), the solution can be written as $\mathbf{v}(\mathbf{r}) = \mathbf{G}(\mathbf{r}) \cdot \mathbf{F}_p$ and $p(\mathbf{r}) = \mathbf{Q}(\mathbf{r}) \cdot \mathbf{F}_p$, which defines the Green tensor $\mathbf{G}(\mathbf{r})$ and pressure vector $\mathbf{Q}(\mathbf{r})$. Their expressions are known up to one integral to be numerically evaluated, see Ref. [25]. In a cylindrical coordinate system (ρ, ϕ, z) where $\hat{\mathbf{n}}$ is taken to be the z axis, we parametrize the fundamental solution as

$$4\pi\eta\mathbf{G}(\mathbf{r}) = A(\rho, z)\hat{\rho}\hat{\rho} + B(\rho, z)(\hat{\rho}\hat{\mathbf{n}} + \hat{\mathbf{n}}\hat{\rho}) + C(\rho, z)\hat{\mathbf{n}}\hat{\mathbf{n}} + D(\rho, z)\hat{\phi}\hat{\phi} \quad (4)$$

and

$$4\pi\mathbf{Q}(\mathbf{r}) = R(\rho, z)\hat{\rho} + Z(\rho, z)\hat{\mathbf{n}}. \quad (5)$$

The precise form of the scalar functions A, B, C, D, R , and Z can be found in Ref. [25], however, for completeness, we also present these functions in Appendix A.

Despite the complicated form of these scalar functions, the short- and long-distance behaviour of the Green’s functions have a simple form [25]. For short distances from the origin, viscous stresses are much larger than the Brinkman force density, and we find the Oseen (or Stokeslet) form

$$\mathbf{G}(\mathbf{r}) \sim \frac{1}{8\pi\eta r} (\mathbf{I} + \hat{\mathbf{r}}\hat{\mathbf{r}}), \quad \rho, z \ll \max(\kappa_{\perp}^{-1}, \kappa_{\parallel}^{-1}). \quad (6)$$

In contrast, for large distances the viscous stresses can be neglected. From the balance of the pressure gradient and the Brinkman damping force density, we find a stretched dipolar form

$$\mathbf{G}(\mathbf{r}) \sim \frac{\kappa_{\parallel}\kappa_{\perp}^2}{4\pi\eta} \left(\frac{3\mathbf{r}\mathbf{r}}{\bar{r}^5} - \frac{1}{\bar{r}^3} \boldsymbol{\kappa}^{-2} \right), \quad \rho, z \gg \max(\kappa_{\perp}^{-1}, \kappa_{\parallel}^{-1}), \quad (7)$$

with scaled coordinate $\bar{r} = \sqrt{(\kappa_{\perp}\rho)^2 + (\kappa_{\parallel}z)^2}$. Note that in contrast to the electrostatic case, the far-field behaviour is not screened, which is a direct result of the incompressibility condition. This is the most transparent for the isotropic case, $\kappa_{\parallel} = \kappa_{\perp}$, for which closed-form expressions (without integrals) exist for the Green’s functions. Here, the tensorial components of $\mathbf{G}(\mathbf{r})$ – defined as the functions h_1 and h_2 in Appendix A – each contain one term that does not decay exponentially [29] and have to be compensated by pressure.

Each velocity field due to a point source can be understood using Eqs. (6) and (7) as limiting situations. Examples of the velocity fields $\mathbf{v}(\mathbf{r})$ for different screening anisotropies and different directions of the force \mathbf{F}_p are shown in Fig. 1. Whereas the near-field solutions ($\kappa r \ll 1$) always correspond to a Stokeslet and the far field to a rescaled source dipole, the intermediate regime can take a complex form. For a sufficiently large ratio $\kappa_{\parallel}/\kappa_{\perp}$, a pair of secondary vortex rings can appear. Their appearance is reminiscent of the Moffatt eddies in a corner [30] or in a cavity [31], as well as toroidal eddies in a pipe [32]. However, in all these examples flow recirculation is caused by confinement and the eddies in a pipe can even disappear in the presence of a BDB fluid with sufficiently strong screening [33]. The appearance of secondary eddies without confinement is therefore a unique feature of an anisotropic BDB fluid.

B. Friction problem of a sphere suspended in an anisotropic porous medium

We consider a sphere of radius a moving with translational velocity \mathbf{U} in a fluid-containing anisotropic porous mass. Since we are interested in the steady motion of the particle, it suffices to consider a sphere in the origin of the laboratory frame. For the corresponding friction problem, we need to solve the boundary value problem given by Eqs. (1) and (2) for $r > a$ and $\mathbf{f} = \mathbf{0}$, supplemented by the boundary conditions $\mathbf{v}(a\hat{\mathbf{r}}) = \mathbf{U}$, and $\mathbf{v}(\mathbf{r}) \rightarrow 0, p(\mathbf{r}) \rightarrow p_{\infty}$ (=constant) for $r \rightarrow \infty$. From $\mathbf{v}(\mathbf{r})$ and $p(\mathbf{r})$ the corresponding hydrodynamic stress tensor can be computed: $\boldsymbol{\sigma} = -p(\mathbf{r})\mathbf{I} + \eta\{\nabla\mathbf{v}(\mathbf{r}) + [\nabla\mathbf{v}(\mathbf{r})]^T\}$, with T denoting the transpose. The force that the particle acts on the fluid is given by

$$\mathbf{F} = \oint_{r=a} \boldsymbol{\sigma}(\mathbf{r}) \cdot d\mathbf{S} = \eta\boldsymbol{\kappa}^2 \cdot \int_{r>a} dV \mathbf{v}(\mathbf{r}), \quad (8)$$

where the surface element $d\mathbf{S}$ points from the fluid to the particle. The second equality follows from the steady-

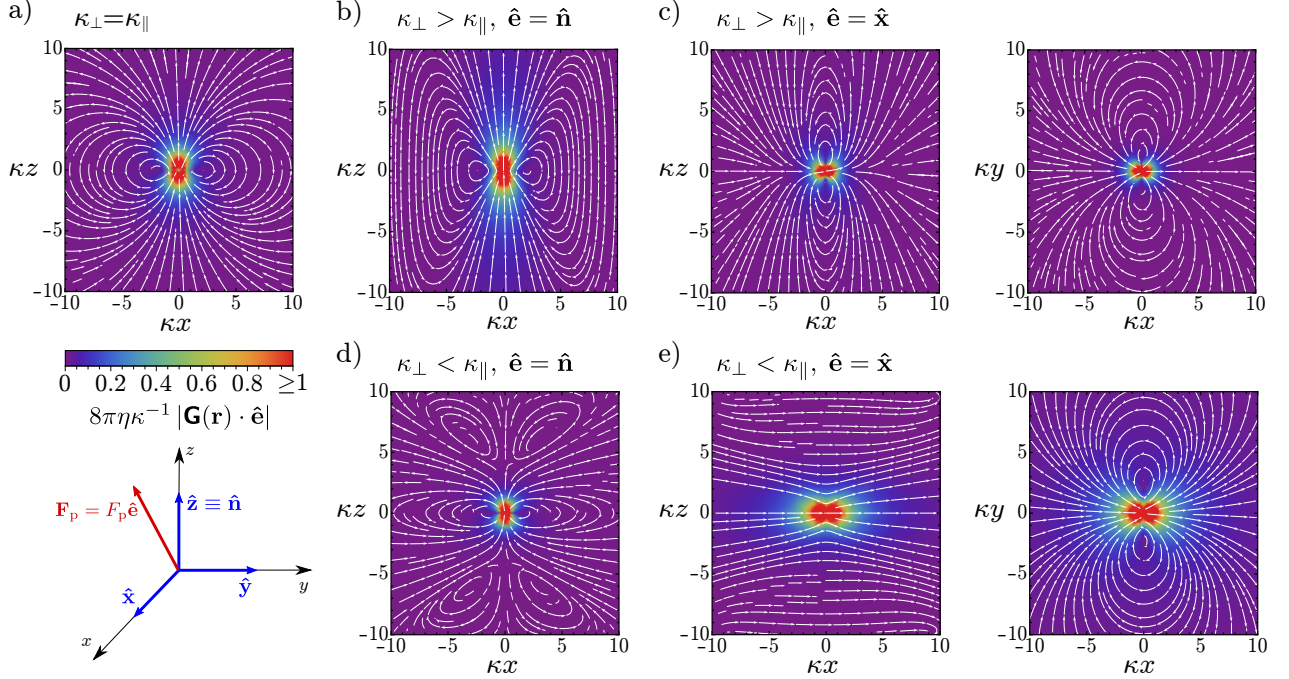


FIG. 1. Streamlines and dimensionless magnitude of the fluid velocity field $\mathbf{v}(\mathbf{r}) = \mathbf{G}(\mathbf{r}) \cdot \mathbf{F}_p$ in response to a point force density with strength $\mathbf{F}_p = F_p \hat{\mathbf{e}}$. The coordinate system and corresponding unit vectors are defined in the lower left panel. (a) Velocity in an isotropic medium. (b,c) Velocity in a medium with stronger transverse screening, $\kappa_{\perp} = 5\kappa_{\parallel}$. (d,e) Velocity in a medium with stronger longitudinal screening $\kappa_{\perp} = (1/5)\kappa_{\parallel}$ (d,e). Panels (a), (b) and (d) show the response to a parallel force, $\hat{\mathbf{e}} = \hat{\mathbf{n}}$ and panels (c) and (e) show the response to a perpendicular force $\hat{\mathbf{e}} = \hat{\mathbf{x}}$ in two different planes. Secondary eddies can appear in the case $\kappa_{\parallel} > \kappa_{\perp}$ and longitudinal force (d).

motion condition, which implies that no net force is acting on the fluid. Therefore, the hydrodynamic drag force $-\mathbf{F}$ can also be computed by considering the force the porous mass exerts on the fluid.

By linearity of Eqs. (1) and (2) we write $\mathbf{F} = \boldsymbol{\zeta} \cdot \mathbf{U}$, where $\boldsymbol{\zeta}$ is the friction tensor. For our axisymmetric problem, it has the form

$$\boldsymbol{\zeta} = \zeta_{\parallel} \hat{\mathbf{n}} \hat{\mathbf{n}} + \zeta_{\perp} (\mathbf{I} - \hat{\mathbf{n}} \hat{\mathbf{n}}), \quad (9)$$

where we defined the longitudinal (transverse) drag coefficient ζ_{\parallel} (ζ_{\perp}) with respect to $\hat{\mathbf{n}}$. Eq. (9) is related to the diffusion tensor via the fluctuation-dissipation theorem, $\mathbf{D} = k_B T \boldsymbol{\zeta}^{-1}$, where k_B is the Boltzmann constant and T temperature. Here, the components of \mathbf{D} describe diffusion along $\hat{\mathbf{n}}$ and in the plane perpendicular to $\hat{\mathbf{n}}$. The diffusion constant related to the mean-squared displacement is given by $\text{Tr}(\mathbf{D})/3$. In Secs. III and IV we will determine $\boldsymbol{\zeta}$ analytically and numerically, respectively.

III. ANALYTICAL RESULTS FOR SMALL ANISOTROPY

In the case of small anisotropy, we will derive an approximate solution by means of the Lorentz reciprocal theorem [34]. The theorem provides an integral iden-

tity between the main problem, for which we choose an anisotropic BDB fluid, and the auxiliary problem, for which we take isotropic BDB flow. In both problems, we treat the interaction with the porous medium as an external force. In this case, the Lorentz reciprocal theorem for a sphere in an unbounded fluid reads [29]

$$\oint_{r=a} \mathbf{v}_0(\mathbf{r}) \cdot [\boldsymbol{\sigma}(\mathbf{r}) \cdot d\mathbf{S}] - \int_{r>a} dV \mathbf{v}_0(\mathbf{r}) \cdot [\nabla \cdot \boldsymbol{\sigma}(\mathbf{r})] = \oint_{r=a} \mathbf{v}(\mathbf{r}) \cdot [\boldsymbol{\sigma}_0(\mathbf{r}) \cdot d\mathbf{S}] - \int_{r>a} dV \mathbf{v}(\mathbf{r}) \cdot [\nabla \cdot \boldsymbol{\sigma}_0(\mathbf{r})] \quad (10)$$

where $\mathbf{v}(\mathbf{r})$ satisfies Eqs. (1)-(3) with stress tensor $\boldsymbol{\sigma}(\mathbf{r})$. The auxiliary problem has a velocity field $\mathbf{v}_0(\mathbf{r})$ and stress tensor $\boldsymbol{\sigma}_0(\mathbf{r})$ and is described by the same equations, but with isotropic shielding tensor $\boldsymbol{\kappa}_0 = \kappa \mathbf{I}$ (with κ to be specified later). Furthermore, we impose the same boundary conditions (i.e., $\mathbf{v}(a\hat{\mathbf{r}}) = \mathbf{v}_0(a\hat{\mathbf{r}}) = \mathbf{U}$).

The force that the sphere exerts on the fluid for the auxiliary system (given by \mathbf{F}_0) and the system of interest (given by \mathbf{F}) then satisfy the relation

$$\mathbf{U} \cdot (\mathbf{F} - \mathbf{F}_0) = \eta \int_{r>a} dV \mathbf{v}_0(\mathbf{r}) \cdot (\boldsymbol{\kappa}^2 - \kappa^2 \mathbf{I}) \cdot \mathbf{v}(\mathbf{r}) \quad (11)$$

where we used the boundary condition on the fluid velocity fields in Eq. (10), that the divergence of the stress

tensor gives the force density acting on the fluid, and that the considered shielding tensors are symmetric. In the isotropic auxiliary system, the friction tensor is analytically known, and we write $\mathbf{F}_0 = \zeta_0(\kappa, a)\mathbf{U}$, with ζ_0 given by

$$\zeta_0(\kappa, a) = 6\pi\eta a \left[1 + \kappa a + \frac{(\kappa a)^2}{9} \right]. \quad (12)$$

Note the factor $1/9$ which is different from the result quoted by Brinkman [9], which has a factor $1/3$ instead. This is a known property of the Brinkman equation: the drag of a moving sphere in a quiescent fluid is different from the drag of a stationary sphere in a fluid with constant ambient velocity [35, 36]. From Eq. (11) we then find the exact relation

$$[\zeta - \zeta_0(\kappa, a)\mathbf{I}] : \mathbf{U}\mathbf{U} = \eta \left[(\bar{\kappa}^2 - \kappa^2)\mathbf{I} + \frac{(\kappa_\perp^2 - \kappa_\parallel^2)}{3}(\mathbf{I} - 3\hat{\mathbf{n}}\hat{\mathbf{n}}) \right] : \int_{r>a} dV \mathbf{v}_0(\mathbf{r})\mathbf{v}(\mathbf{r}), \quad (13)$$

with $\bar{\kappa}^2 = (2\kappa_\perp^2 + \kappa_\parallel^2)/3$. However, there is no analytical expression for $\mathbf{v}(\mathbf{r})$. We obtain an approximate expression in two steps. First, we take the approximation $\mathbf{v}(\mathbf{r}) \approx \mathbf{v}_0(\mathbf{r})$ in Eq. (13). We thus need to compute the dyadic integral

$$\int_{r>a} dV \mathbf{v}_0(\mathbf{r})\mathbf{v}_0(\mathbf{r}) = c_1\mathbf{U}\mathbf{U} + c_2U^2\mathbf{I}, \quad (14)$$

where the structure of the integral follows from symmetry with $U = |\mathbf{U}|$. The coefficients c_1 and c_2 can be explicitly evaluated (see Appendix B). Note that c_2 does not contribute to the second term of the RHS in Eq. (13) due to the double contraction with a traceless tensor. In the second step, we choose $\kappa = (2\kappa_\perp + \kappa_\parallel)/3$ and expand Eq. (13) using

$$\epsilon = \frac{\kappa_\perp - \kappa_\parallel}{\kappa} \quad (15)$$

as a small parameter by using $\kappa_\perp = \kappa(1 + \epsilon/3)$ and $\kappa_\parallel = \kappa(1 - 2\epsilon/3)$. Our motivation for selecting this reference system is that $\bar{\kappa}^2 - \kappa^2 = \mathcal{O}(\epsilon^2)$, and therefore we can neglect the first term in Eq. (13). We find to linear order in ϵ ,

$$\zeta - \zeta_0(\kappa, a)\mathbf{I} = 6\pi\eta a \frac{63 + 2\kappa a}{270} (\kappa_\perp - \kappa_\parallel)a(\mathbf{I} - 3\hat{\mathbf{n}}\hat{\mathbf{n}}) + \mathcal{O}(\epsilon^2). \quad (16)$$

An interesting corollary of our result is that $\text{Tr}(\zeta - \zeta_0\mathbf{I}) = \mathcal{O}(\epsilon^2)$, which suggests that there is a large parameter regime for which the diffusion constant is well approximated by the result from an isotropic analysis with κ as inverse screening length. A comparison between the linear approximation and full numerical results (see next section) is shown in Fig. 2. Surprisingly, we see that our linear approximation Eq. (16) has a large range of applicability, even when $|\epsilon|$ is on the order of unity. Deviations with the numerical result only occur when κa is sufficiently large. The precise regime where Eq. (16) is valid will be further analysed in Sec. IV.

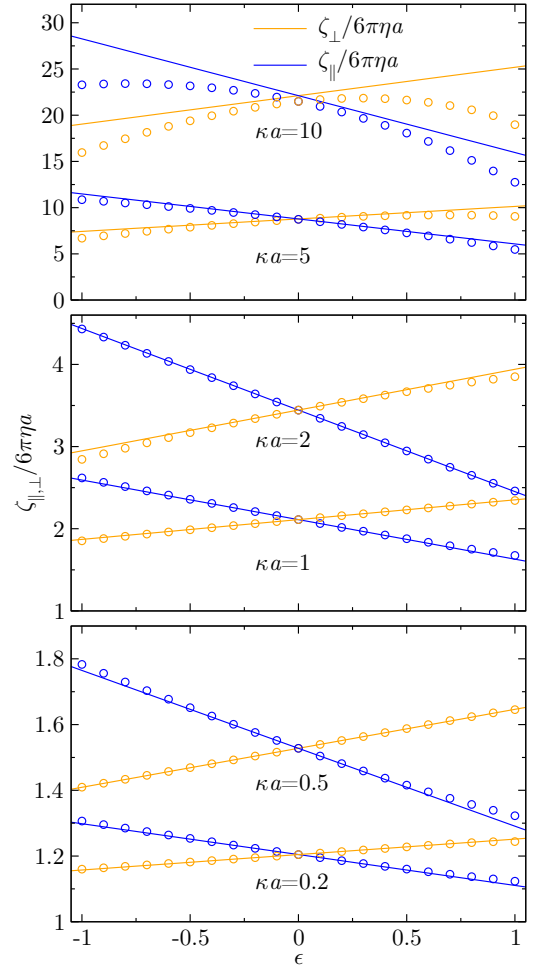


FIG. 2. Transverse (orange) and longitudinal (blue) drag coefficients as a result of the linear approximation (Eq. (16), solid lines) and numerical results using the BEM (circles).

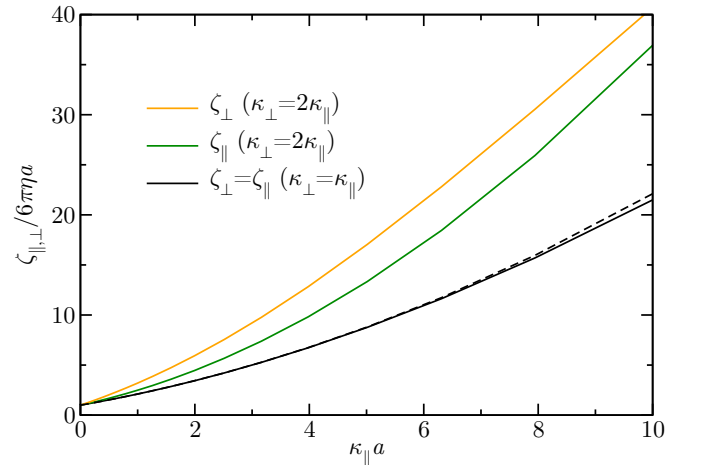


FIG. 3. Transverse (ζ_\perp) and longitudinal (ζ_\parallel) drag coefficients, obtained using the boundary element method. The black line shows the result for an isotropic medium (with the dashed line showing the exact analytical result, Eq. (12)) and the orange/green lines for a medium with $\kappa_\perp = 2\kappa_\parallel$.

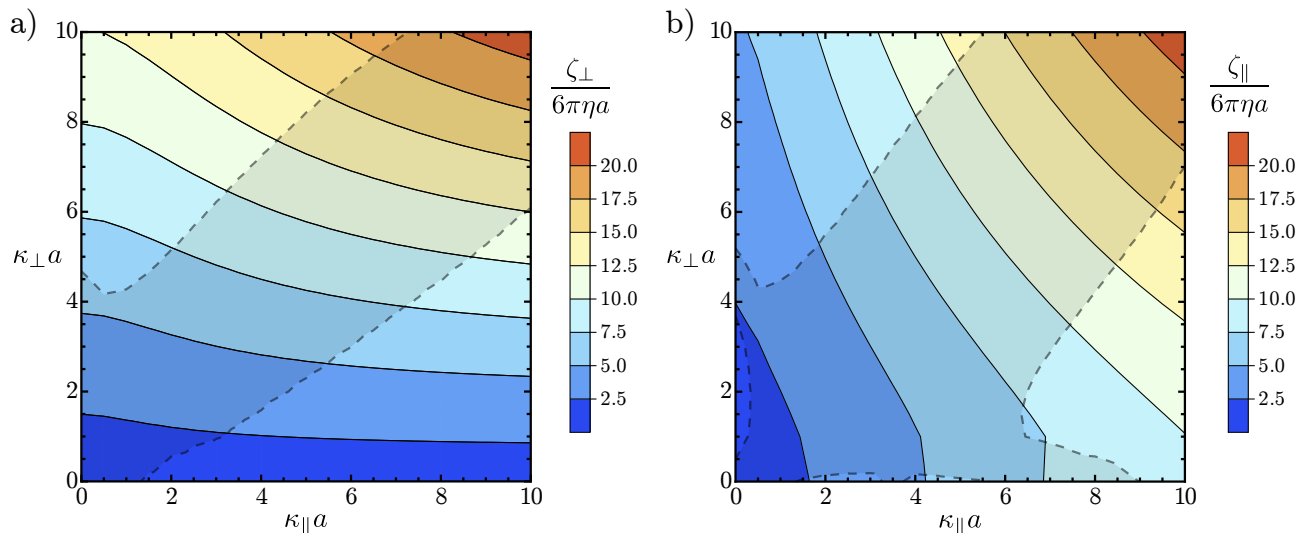


FIG. 4. Transverse (a) and longitudinal (b) drag coefficients, determined numerically using the boundary element method. The shaded region shows the parameter range for which the discrepancy between the linear approximation and the numerical result lies below 5%.

IV. NUMERICAL DETERMINATION OF THE FRICTION TENSOR

The numerical solution consists of numerically integrating the expressions for the Green's functions (Eqs. (A1)-(A4) and (A8)-(A11)) and then solving the flow problem with the Boundary Element Method (BEM). We carried out the integration over t or s using the adaptive integration routine QAGIU from GNU Scientific Library (GSL). The obtained Green's functions were then used by a BEM solver using a single-layer formulation (adapted from the function `prtcl3d`, which is part of the BEMLIB package [26]). The surface of the spherical particle was discretised with 512 triangular elements. Finally, the obtained drag coefficients were reduced by the internal contribution, $(4/3)\pi\eta\kappa_{\parallel}^2a^3$ and $(4/3)\pi\eta\kappa_{\perp}^2a^3$ for the longitudinal and transverse drag, respectively, which is included in the result of a single-layer solution.

The computed drag coefficients, ζ_{\parallel} and ζ_{\perp} , are shown in Fig. 3 for two values of the ratio $\kappa_{\perp}/\kappa_{\parallel}$. In the isotropic case ($\kappa_{\perp} = \kappa_{\parallel}$), the results show good agreement with the exact analytical expression (Eq. (12)). A minor deviation is visible at large values of $\kappa_{\parallel}a$, where the screening length becomes smaller than the size of a boundary element.

The whole range of numerical values of the drag coefficients ζ_{\parallel} and ζ_{\perp} is shown by the contour plots in Fig. 4. Along with the linear plots in Fig. 2, the results show that there is a wide parameter regime—indicated by the shaded region—where the approximate result, given by Eq. (16), agrees with the numerical value with a discrepancy smaller than 5%.

V. CONCLUDING REMARKS

In this work, we have analysed the drag force on a translating spherical particle in a quiescent anisotropic BDB with axisymmetric shielding tensor. We numerically determined the components of the friction tensor by using the BEM, from which the diffusion tensor can be inferred. Furthermore, we have provided an approximate analytical formula that is valid in a wide range of the parameter space, which could be useful for experimentalists or as an input for theoretical models.

The diffusion tensor considered in this work (which can be extracted from the friction tensor) is that of a sphere in a static anisotropic porous medium. For the experiments listed in the introduction (Refs. [17–19]), the results should, therefore, be interpreted as a short-time diffusion tensor, whereas typically the long-time diffusion coefficients are measured. It would be interesting to expand the effective nematic theory analysed in Refs. [17–21] to include the effects of anisotropic hydrodynamic screening using our results as an input. Since the crowders are rod-shaped, it corresponds to the case where $\kappa_{\perp} > \kappa_{\parallel}$. The opposite case, $\kappa_{\perp} < \kappa_{\parallel}$, would correspond to a nematic system where the short axis of the particles are nematically ordered, which is the case, for example, for disc-like particles. However, certain experiments are essential for making a sensible comparison of theory with measurements. For example, an important consistency check is obtained by performing measurements for various tracer sizes, to check whether the extracted screening lengths are independent of the probe size, as it is a property of the nematic medium. Such a consistency check is currently lacking for the existing experiments.

Beyond the scope of these experiments, our results have general merit for the study of anisotropic porous me-

dia within the BDB framework, generalizing the classical work by Brinkman [9] to the axisymmetric case. Specifically, our results could be useful for problems where diffusion through porous media play an important role, like in the charging kinetics of supercapacitors [37] or heterogeneous catalysis [38]. Another possible direction is to investigate the interplay between anisotropic hydrodynamic screening with anisotropic electrostatic screening [39] for the diffusion or electrophoresis of charged particles, which is currently only touched upon for the isotropic case [19].

ACKNOWLEDGEMENTS

A. V. acknowledges funding from the Slovenian Research and Innovation Agency, grant no. P1-0099. J. C. E. acknowledges funding from the National Science Centre, Poland, within the SONATA BIS grant no. 2023/50/E/ST3/00452/R.

Appendix A: Scalar functions for parametrizing the fundamental solution

Here, we list the scalar functions defined in the parametrization of the fundamental solution, see Eqs. (4) and (5). We need to distinguish the cases $\kappa_\perp > \kappa_\parallel$ and $\kappa_\perp < \kappa_\parallel$. Results are taken from Ref. [25], where only the cases for $z > 0$ were presented. Here, we present expressions for general z .

The $\kappa_\perp > \kappa_\parallel$ case

The functions for $\kappa_\perp > \kappa_\parallel$ are given by

$$A(\rho, z) = \frac{1}{\kappa_\perp \rho^2} (e^{-\kappa_\perp |z|} - e^{-\kappa_\perp r}) + \int_0^\infty dt \frac{t}{\Delta_b(t)} \left[b_+(t) e^{-b_+(t)|z|} - b_-(t) e^{-b_-(t)|z|} \right] J_1'(t\rho), \quad (\text{A1})$$

$$B(\rho, z) = -\text{sgn}(z) \int_0^\infty dt \frac{t^2}{\Delta_b(t)} \left[e^{-b_+(t)|z|} - e^{-b_-(t)|z|} \right] J_1(t\rho), \quad (\text{A2})$$

$$C(\rho, z) = - \int_0^\infty dt \frac{t^3}{\Delta_b(t)} \left[\frac{e^{-b_+(t)|z|}}{b_+(t)} - \frac{e^{-b_-(t)|z|}}{b_-(t)} \right] J_0(t\rho), \quad (\text{A3})$$

$$D(\rho, z) = \frac{1}{r} e^{-\kappa_\perp r} - \frac{1}{\kappa_\perp \rho^2} (e^{-\kappa_\perp |z|} - e^{-\kappa_\perp r}) + \int_0^\infty dt \frac{t}{\Delta_b(t)} \left[b_+(t) e^{-b_+(t)|z|} - b_-(t) e^{-b_-(t)|z|} \right] \frac{J_1(t\rho)}{t\rho}, \quad (\text{A4})$$

$$R(\rho, z) = \frac{1}{2} \int_0^\infty dt \frac{t^2}{\Delta_b(t)} \left\{ [\Delta_b(t) - 2\kappa_\parallel^2 + \kappa_\perp^2] \frac{e^{-b_+(t)|z|}}{b_+(t)} + [\Delta_b(t) + 2\kappa_\parallel^2 - \kappa_\perp^2] \frac{e^{-b_-(t)|z|}}{b_-(t)} \right\} J_1(t\rho), \quad (\text{A5})$$

$$Z(\rho, z) = \frac{1}{2} \text{sgn}(z) \int_0^\infty dt \frac{t}{\Delta_b(t)} \left\{ [\Delta_b(t) - \kappa_\perp^2] e^{-b_+(t)|z|} + [\Delta_b(t) + \kappa_\perp^2] e^{-b_-(t)|z|} \right\} J_0(t\rho), \quad (\text{A6})$$

where a prime denotes differentiation with respect to the argument and J_n is the n th-order Bessel function of the first kind. Furthermore, we have that

$$b_\pm(t)^2 = t^2 + \frac{1}{2} \left(\kappa_\perp^2 \pm \sqrt{\kappa_\perp^4 + 4(\kappa_\perp^2 - \kappa_\parallel^2)t^2} \right) \geq 0 \quad (\text{A7})$$

and $\Delta_b(t) = b_+(t)^2 - b_-(t)^2$.

The $\kappa_\perp < \kappa_\parallel$ case

The functions for $\kappa_\perp < \kappa_\parallel$ are given by

$$A(\rho, z) = -\frac{e^{-\kappa_\perp r}}{\kappa_\perp \rho^2} + \frac{2}{\pi} \int_0^\infty ds \frac{s^2 \cos(sz)}{\Delta_c(s)} [K_1'(c_+(s)\rho) - K_1'(c_-(s)\rho)], \quad (\text{A8})$$

$$B(\rho, z) = -\frac{2}{\pi} \int_0^\infty ds \frac{s \sin(sz)}{\Delta_c(s)} [c_+(s) K_1(c_+(s)\rho) - c_-(s) K_1(c_-(s)\rho)], \quad (\text{A9})$$

$$C(\rho, z) = \frac{2}{\pi} \int_0^\infty ds \frac{\cos(sz)}{\Delta_c(s)} [c_+(s)^2 K_0(c_+(s)\rho) - c_-(s)^2 K_0(c_-(s)\rho)], \quad (\text{A10})$$

$$D(\rho, z) = \left(\frac{1}{r} + \frac{1}{\kappa_\perp \rho^2} \right) e^{-\kappa_\perp r} + \frac{2}{\pi} \int_0^\infty ds \frac{s^2 \cos(sz)}{\Delta_c(s)} \left[\frac{K_1(c_+(s)\rho)}{c_+(s)\rho} - \frac{K_1(c_-(s)\rho)}{c_-(s)\rho} \right], \quad (\text{A11})$$

$$R(\rho, z) = \frac{1}{\pi} \int_0^\infty ds \frac{\cos(sz)}{\Delta_c(s)} \left\{ [\Delta_c(s) - \kappa_\parallel^2] c_+(s) K_1(c_+(s)\rho) + [\Delta_c(s) + \kappa_\parallel^2] c_-(s) K_1(c_-(s)\rho) \right\}, \quad (\text{A12})$$

$$Z(\rho, z) = \frac{1}{\pi} \int_0^\infty ds \frac{s \sin(sz)}{\Delta_c(s)} \left\{ [\Delta_c(s) + \kappa_\parallel^2 - 2\kappa_\perp^2] K_0(c_+(s)\rho) + [\Delta_c(s) - \kappa_\parallel^2 + 2\kappa_\perp^2] K_0(c_-(s)\rho) \right\}, \quad (\text{A13})$$

where K_n is the n th-order modified Bessel function of the second kind. Furthermore, we have defined the auxiliary functions

$$c_\pm(s)^2 = s^2 + \frac{1}{2} \left(\kappa_\parallel^2 \pm \sqrt{\kappa_\parallel^4 + 4(\kappa_\parallel^2 - \kappa_\perp)^2 s^2} \right) \geq 0 \quad (\text{A14})$$

and $\Delta_c(s) = c_+(s)^2 - c_-(s)^2$.

The $\kappa_\perp = \kappa_\parallel$ case

The formulas in the case of anisotropic hydrodynamic screening can be explicitly evaluated for $\kappa_\perp = \kappa_\parallel$, for which the formulas for $\kappa_\perp < \kappa_\parallel$ and $\kappa_\perp > \kappa_\parallel$ give the same result. In this case, the fundamental solution takes the form

$$\mathbf{G}(\mathbf{r}) = \frac{1}{4\pi\eta r} [h_1(\kappa r)\mathbf{I} + h_2(\kappa r)\hat{\mathbf{r}}\hat{\mathbf{r}}] \quad (\text{A15})$$

and

$$\mathbf{Q}(\mathbf{r}) = \frac{1}{4\pi r^2} \hat{\mathbf{r}}. \quad (\text{A16})$$

Here, we defined

$$h_1(x) = -\frac{1}{x^2} + \left(1 + \frac{1}{x} + \frac{1}{x^2} \right) e^{-x}, \quad (\text{A17})$$

$$h_2(x) = \frac{3}{x^2} - \left(1 + \frac{3}{x} + \frac{3}{x^2} \right) e^{-x}. \quad (\text{A18})$$

Note that all the expressions presented in this Appendix will give the dipolar form (Eq. (7)) in the far-field limit, as was shown in Ref. [25]. However, there was a printing error in this manuscript. Eq. 65 in Ref. [25] should read

$$C_D(\rho, z) = -\frac{\kappa_\perp^2}{\kappa_\parallel r^3} + 3\kappa_\perp^2 \kappa_\parallel \frac{z^2}{r^5}. \quad (\text{A19})$$

Appendix B: Evaluation of coefficients c_1 and c_2

This Appendix provides the details for evaluating Eq. (14). We parametrize the velocity field as

$$\mathbf{v}_0(\mathbf{r}) = [F(r)\mathbf{I} + H(r)\hat{\mathbf{r}}\hat{\mathbf{r}}] \cdot \mathbf{U}, \quad (\text{B1})$$

with

$$F(r) = \frac{3}{2} \left(\frac{\kappa a e^{\kappa a}}{(\kappa r)^3} \{ [1 + \kappa r + (\kappa r)^2] e^{-\kappa r} - 1 \} + \frac{a^3}{r^3} \frac{3e^{\kappa a} - 3 - 3\kappa a - (\kappa a)^2}{3(\kappa a)^2} \right) \quad (\text{B2})$$

and

$$H(r) = \frac{3}{2} \left(\frac{\kappa a e^{\kappa a}}{(\kappa r)^3} \{ 3 - [3 + 3\kappa r + (\kappa r)^2] e^{-\kappa r} \} - \frac{a^3}{r^3} \frac{3e^{\kappa a} - 3 - 3\kappa a - (\kappa a)^2}{(\kappa a)^2} \right), \quad (\text{B3})$$

as can be derived by directly evaluating the singularity form presented in Sec. 6.2.1 of Ref. [29]. Insertion of Eq. (B1) into Eq. (14) gives $\int_{r>a} dV \mathbf{v}_0(\mathbf{r}) \mathbf{v}_0(\mathbf{r}) = \mathbf{U} \cdot \mathbf{A} \cdot \mathbf{U}$, with rank 4 tensor

$$\mathbf{A} = \int_{r>a} dV [F(r)^2 \mathbf{I} \mathbf{I} + F(r)H(r)(\hat{\mathbf{r}}\hat{\mathbf{r}} + \hat{\mathbf{r}}\hat{\mathbf{r}}) + H(r)^2 \hat{\mathbf{r}}\hat{\mathbf{r}}\hat{\mathbf{r}}\hat{\mathbf{r}}]. \quad (\text{B4})$$

Passing to spherical coordinates, the angular integrations can be performed with

$$\int_{\mathcal{S}^2} dS \xi_\alpha \xi_\beta = \frac{4\pi}{3} \delta_{\alpha\beta}, \quad (\text{B5})$$

$$\int_{\mathcal{S}^2} dS \xi_\alpha \xi_\beta \xi_\gamma \xi_\sigma = \frac{4\pi}{15} (\delta_{\alpha\beta} \delta_{\gamma\sigma} + \delta_{\alpha\gamma} \delta_{\beta\sigma} + \delta_{\alpha\sigma} \delta_{\beta\gamma}), \quad (\text{B6})$$

with $[\hat{\mathbf{r}}]_\alpha = \xi_\alpha$ and \mathcal{S}^2 denoting the two-dimensional unit sphere. We can read off the coefficients by comparing them with Eq. (14). We find

$$c_1 = 4\pi \int_a^\infty dr r^2 \left[F(r)^2 + \frac{2}{3} F(r)H(r) + \frac{2}{15} H(r)^2 \right] = \frac{a^2 \pi (63 + 2\kappa a)}{30\kappa} \quad (\text{B7})$$

and

$$c_2 = \frac{4\pi}{15} \int_a^\infty dr r^2 H(r)^2 = \frac{a^2(3 + 2\kappa a)\pi}{10\kappa}. \quad (\text{B8})$$

Interestingly, in c_1 and c_2 , all terms containing exponentials and exponential integrals are canceled. This can be understood by applying the Lorentz reciprocal theorem again. This time, we take two isotropic systems with inverse screening lengths $\kappa + \delta$ and κ , respectively, with all other conditions the same in both systems. Then,

$$\begin{aligned} \mathbf{U} \cdot [\mathbf{F}_0(\kappa + \delta, a) - \mathbf{F}_0(\kappa, a)] \\ = (2\kappa + \delta)\eta\delta \int_{r>a} dV \mathbf{v}_0(\mathbf{r}; \kappa + \delta, a) \cdot \mathbf{v}_0(\mathbf{r}; \kappa, a), \end{aligned} \quad (\text{B9})$$

where we write the explicit parameters as an argument

to distinguish what isotropic system is used. Now take $\delta \rightarrow 0$ and we find

$$\mathbf{U} \cdot \frac{\partial}{\partial \kappa} \mathbf{F}_0(\kappa, a) = 2\kappa\eta \int_{r>a} dV \mathbf{v}_0(\mathbf{r}; \kappa, a) \cdot \mathbf{v}_0(\mathbf{r}; \kappa, a). \quad (\text{B10})$$

However, $\mathbf{F}_0(\kappa, a) = \zeta_0(\kappa, a)\mathbf{U}$ and using the parametrization of Eq. (14), we find the exact relation

$$\frac{\partial}{\partial \kappa} \zeta_0(\kappa, a) = 2\kappa\eta[c_1(\kappa, a) + 3c_2(\kappa, a)]. \quad (\text{B11})$$

The left-hand side, determined by using Eq. (12), is consistent with the values found for the coefficients Eqs. (B7) and (B8).

-
- [1] T. Kühn, T. O. Ihalainen, J. Hyväluoma, N. Dross, S. F. Willman, J. Langowski, M. Vihinen-Ranta, and J. Timonen, Protein diffusion in mammalian cell cytoplasm, *PLoS ONE* **6**, e22962 (2011).
 - [2] N. Boon and R. van Roij, Charge reversal of moisturous porous silica colloids by take-up of protons, *J. Colloid Interface Sci.* **385**, 66 (2012).
 - [3] E. Moeendarbary, L. Valon, M. Fritzsche, A. R. Harris, D. A. Moulding, A. J. Thrasher, E. Stride, L. Mahadevan, and G. T. Charras, The cytoplasm of living cells behaves as a poroelastic material, *Nat. Mater.* **12**, 253 (2013).
 - [4] E. Sasaki, D. Böhringer, M. Van de Waterbeemd, M. Leibundgut, R. Zschoche, A. J. Heck, N. Ban, and D. Hilvert, Structure and assembly of scalable porous protein cages, *Nat. Commun.* **8**, 14663 (2017).
 - [5] J. Severn, T. Vacus, and E. Lauga, Fluid mechanics of sarcomeres as porous media, *Soft Matter* **21**, 2849 (2025).
 - [6] R. Raccis, A. Nikoubashman, M. Retsch, U. Jonas, K. Koynov, H.-J. Butt, C. N. Likos, and G. Fytas, Confined diffusion in periodic porous nanostructures, *ACS Nano* **5**, 4607 (2011).
 - [7] M. J. Blunt, B. Bijeljic, H. Dong, O. Gharbi, S. Iglauer, P. Mostaghimi, A. Paluszny, and C. Pentland, Pore-scale imaging and modelling, *Adv. Water Resour.* **51**, 197 (2013).
 - [8] S. Aramideh, P. P. Vlachos, and A. M. Ardekani, Pore-scale statistics of flow and transport through porous media, *Phys. Rev. E* **98**, 013104 (2018).
 - [9] H. C. Brinkman, A calculation of the viscous force exerted by a flowing fluid on a dense swarm of particles, *Appl. Sci. Res.* **A1**, 27 (1949).
 - [10] P. Debye and A. M. Bueche, Intrinsic viscosity, diffusion, and sedimentation rate of polymers in solution, *J. Chem. Phys.* **16**, 573 (1948).
 - [11] L. Durlinsky and J. F. Brady, Analysis of the Brinkman equation as a model for flow in porous media, *Phys. Fluids* **30**, 3329 (1987).
 - [12] J. Feng, P. Ganatos, and S. Weinbaum, Motion of a sphere near planar confining boundaries in a Brinkman medium, *J. Fluid Mech.* **375**, 265–296 (1998).
 - [13] Y. Uematsu, Electrophoresis of electrically neutral porous spheres induced by selective affinity of ions, *Phys. Rev. E* **91**, 022303 (2015).
 - [14] M. Gruca, M. Bukowicki, and M. L. Ekiel-Jeżewska, Brinkman-medium resistance hampers periodic motions of sedimenting particles, *Acta Mech.* **236**, 837 (2024).
 - [15] J. Yang and S. Lee, Effect of anisotropy on transport phenomena in anisotropic porous media, *Int. J. Heat Mass Transf.* **42**, 2673 (1999).
 - [16] S. L. Dettmer, S. Pagliara, K. Misiunas, and U. F. Keyser, Anisotropic diffusion of spherical particles in closely confining microchannels, *Phys. Rev. E* **89**, 062305 (2014).
 - [17] K. Kang, J. Gapinski, M. P. Lettinga, J. Buitenhuis, G. Meier, M. Ratajczyk, J. K. G. Dhont, and A. Patkowski, Diffusion of spheres in crowded suspensions of rods, *J. Chem. Phys.* **122**, 044905 (2005).
 - [18] K. Kang, A. Wilk, J. Buitenhuis, A. Patkowski, and J. K. G. Dhont, Diffusion of spheres in isotropic and nematic suspensions of rods, *J. Chem. Phys.* **124**, 044907 (2006).
 - [19] K. Kang, A. Wilk, A. Patkowski, and J. K. G. Dhont, Diffusion of spheres in isotropic and nematic networks of rods: Electrostatic interactions and hydrodynamic screening, *J. Chem. Phys.* **126**, 214501 (2007).
 - [20] J. Guzowski, B. Cichocki, E. Wajnryb, and G. C. Abade, The short-time self-diffusion coefficient of a sphere in a suspension of rigid rods, *J. Chem. Phys.* **128**, 094502 (2008).
 - [21] B. Cichocki and M. L. Ekiel-Jeżewska, Self-diffusion of a sphere in an effective medium of rods, *J. Chem. Phys.* **130**, 214902 (2009).
 - [22] F. Babayekhorasani, D. E. Dunstan, R. Krishnamoorti, and J. C. Conrad, Nanoparticle diffusion in crowded and confined media, *Soft Matter* **12**, 8407 (2016).
 - [23] J. Bear and Y. Bachmat, *Introduction to modeling of transport phenomena in porous media*, Theory and Applications of Transport in Porous Media, Vol. 4 (Springer Science & Business Media, 1990).
 - [24] M. Kohr, G. P. R. Sekhar, and J. R. Blake, Green's function of the Brinkman equation in a 2D anisotropic case,

- IMA J. Appl. Math. **73**, 374 (2007).
- [25] B. Cichocki and M. L. Ekiel-Jeżewska, Green tensors for Debye–Bücher–Brinkman equations generalized for axisymmetric medium, *J. Math. Phys.* **51**, 103101 (2010).
- [26] C. Pozrikidis, *A practical guide to boundary element methods with the software library BEMLIB* (CRC Press, 2002).
- [27] H. Darcy, *Les fontaines publiques de la ville de Dijon: exposition et application des principes à suivre et des formules à employer dans les questions de distribution d'eau* (Dalmont, Paris, 1856).
- [28] S. Whitaker, Flow in porous media I: A theoretical derivation of Darcy's law, *Transp. Porous Med.* **151**, 3 (1986).
- [29] S. Kim and S. J. Karrila, *Microhydrodynamics: principles and selected applications* (Courier Corporation, 2013).
- [30] H. K. Moffatt, Viscous and resistive eddies near a sharp corner, *J. Fluid Mech.* **18**, 1 (1964).
- [31] J. J. L. Higdon, Stokes flow in arbitrary two-dimensional domains: shear flow over ridges and cavities, *J. Fluid Mech.* **159**, 195 (1985).
- [32] J. R. Blake, On the generation of viscous toroidal eddies in a cylinder, *J. Fluid Mech.* **95**, 209 (1979).
- [33] A. Daddi-Moussa-Ider and A. Vilfan, On force balance in Brinkman fluids under confinement, *J. Fluid Mech.* **1008**, A11 (2025).
- [34] H. Masoud and H. A. Stone, The reciprocal theorem in fluid dynamics and transport phenomena, *J. Fluid Mech.* **879**, P1 (2019).
- [35] I. D. Howells, Drag due to the motion of a Newtonian fluid through a sparse random array of small fixed rigid objects, *J. Fluid Mech.* **64**, 449 (1974).
- [36] Y. E. Solomentsev and J. L. Anderson, Rotation of a sphere in Brinkman fluids, *Phys. Fluids* **8**, 1119 (1996).
- [37] F. Henrique, P. J. Żuk, and A. Gupta, A network model to predict ionic transport in porous materials, *Proc. Natl. Acad. Sci. U.S.A.* **121**, e2401656121 (2024).
- [38] R. Gounder and M. E. Davis, Beyond shape selective catalysis with zeolites: Hydrophobic void spaces in zeolites enable catalysis in liquid water, *AIChE J.* **59**, 3349 (2013).
- [39] J. C. Everts, B. Senyuk, H. Mundoor, M. Ravník, and I. I. Smalyukh, Anisotropic electrostatic screening of charged colloids in nematic solvents, *Sci. Adv.* **7**, eabd0662 (2021).